

## Scaling of thermal hysteresis at nematic-smectic-A phase transition in a binary mixture

Sevtap Yıldız,<sup>1</sup> Önder Pekcan,<sup>1</sup> A. Nihat Berker,<sup>1,2,3</sup> and Haluk Özbek<sup>1,2,\*</sup><sup>1</sup>Department of Physics, Istanbul Technical University, 34469 Maslak, Istanbul, Turkey<sup>2</sup>Feza Gürsey Research Center for Basic Science, Çengelköy, Istanbul 81220, Turkey<sup>3</sup>Department of Physics, Massachusetts Institute of Technology, Cambridge, Massachusetts 02139, USA

(Received 14 July 2003; published 24 March 2004)

The photon transmission method was applied to study the scaling of thermal hysteresis at the nematic-smectic-A transition in a binary mixture of 4-ethoxy-4'-(6-vinyloxyhexyloxy) azobenzene monomer, smectogen, and 4-hexoxy-3'-methyl-4'-(6-acryloyloxyhexyloxy) azobenzene. The thermal hysteresis loops were obtained under linearly varying temperature. It has been found that the area  $A$  of the hysteresis loops scales with the temperature scanning rate  $R$  as  $A = A_0 + bR^n$  with the exponent  $n$  equal to 0.692, which is consistent with the  $(\Phi^2)^3$  field theoretical model value within the experimental resolution.

DOI: 10.1103/PhysRevE.69.031705

PACS number(s): 64.70.Md, 61.30.Eb, 05.70.Fh, 64.60.Cn

## I. INTRODUCTION

Although hysteresis is a ubiquitous phenomenon in first-order phase transitions, it is a complex process of a dynamic and nonlinear nature which eludes serious treatment both experimentally and theoretically. However, phase transitions driven by a time-dependent external field have recently received considerable interest. Theoretical [1–11] and experimental [12,13] studies have demonstrated that the area  $A$  of the hysteresis loops can obey the scaling form

$$A \approx H_0^\alpha \Omega^\beta \quad (1)$$

for the amplitude  $H_0$  and frequency  $\Omega$  of the applied field. Rao *et al.* [1,2], using a time-dependent Ginzburg-Landau theory of a nonconserved order parameter in large- $N$  limit with a periodic magnetic field, obtained hysteresis loops and the area scaling which is universal for both  $O(N)$ -symmetric  $(\Phi^2)^2$  and  $(\Phi^2)^3$  models. In addition to magnetic hysteresis, thermal hysteresis has also been investigated preliminarily by Rao and Pandit [2] in the  $(\Phi^2)^3$  model. The areas of the thermal hysteresis loops also scale with the amplitude for low values of the periodically oscillating temperature. But the value of the exponent  $\alpha$  is different from the one for magnetic hysteresis loops. It should be noted that, experimentally, a more easily realizable way of varying the temperature is by changing it linearly, rather than periodically. Zhong and Zhang [11] obtained the thermal hysteresis loops under linearly varying temperature by using  $(\Phi^2)^3$  model with  $O(N)$  symmetry. They showed that the enclosed areas  $A$  of the hysteresis loops scale with the rate of temperature scanning  $R$  as

$$A = A_0 + bR^n, \quad (2)$$

where  $n$ , the scaling exponent, approaches two thirds which is universal for both the mean-field and field theoretical models concerned,  $A_0$  and  $b$  are constants. Furthermore, thermal hysteresis has been studied experimentally in various sys-

tems including liquid crystals [14–16], ferromagnetic single crystals [17], and  $\kappa$ -carrageenan-water system [18,19]. To the best of our knowledge, there has not been any systematic experimental study of scaling of thermal hysteresis with temperature scanning rate in liquid crystalline materials. In this work, we present experimental results of thermal hysteretic behavior of a binary mixture of 4-ethoxy-4'-(6-vinyloxyhexyloxy) azobenzene monomer (VE), which is smectogen, and 4-hexoxy-3'-methyl-4'-(6-acryloyloxyhexyloxy) azobenzene monomer (AH), which by itself exhibits no liquid crystalline behavior. We study how the shape and area of the hysteresis loops depend on the scanning rate of the linearly varying temperature during the nematic ( $N$ )-smectic-A (Sm-A) transition by using *in situ* ultraviolet/visible (UV/vis) photon transmission method which has previously been described [20–22].

## II. EXPERIMENT

AH and VE monomers were synthesized by Serhatlı and Serhatlı at the Chemistry Department at ITU. Details are reported in Refs. [23] for the former and [24] for the latter. The structural formula of VE and AH are shown in Fig. 1. The monomers were used without additional purification after having been synthesized. The liquid-crystalline binary

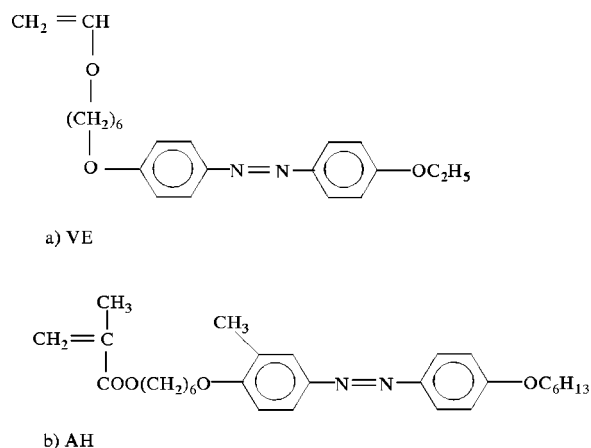


FIG. 1. The structural formula of (a) VE, (b) AH.

\*E-mail address: hozbek@itu.edu.tr

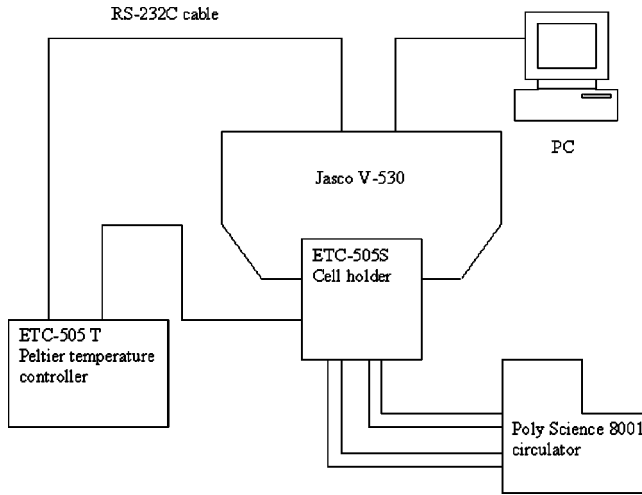


FIG. 2. The block diagram of the experimental setup.

mixture samples were sandwiched separately between two glass plates with Mylar spacers to define the cell thickness ( $\approx 20 \mu\text{m}$ ). The binary mixture preparation has been described elsewhere [25]. The reference surfaces of sandwiched-cell samples were cleaned carefully by using alcohol and acetone, then they were washed by deionized and bidistilled water in an ultrasonic bath. Sandwiched cells were filled by capillary action with the liquid-crystalline binary mixtures. This was done at temperatures above the clearing point to prevent flow alignment of the director. The planar orientation was achieved by rubbing the surfaces of the sandwiched cells with diamond paste in order to avoid multidomain structure. Planar orientation of the smectic phase was achieved by cooling down the preliminary oriented nematic phase.

*In situ* photon transmission measurements were performed at 750 nm wavelength using a Jasco V-530 UV/Vis spectrophotometer in time-course mode. The binary mixture samples were separately placed within the spectrophotometer and another glass plate was used as a standard for all transmitted photon intensity measurements. A background count was carried out using two glass plates before *in situ* measurements. The temperature was measured using an ETC-505T Peltier temperature controller unit equipped with an ETC-505S Peltier thermostatted cell holder and with a Poly Science 8001 programmable circulator. The linear dependence of temperature on time was confirmed by the time-temperature calibration curve performed by DMA-509 DNA melting software package. The block diagram of the experimental setup is shown in Fig. 2. We identified the structure of the mesophases by optical microscopy using a polarizing microscope Olympus BHSP.

### III. RESULTS AND DISCUSSION

The thermal hysteresis loops were obtained by monitoring the transmitted photon intensity  $I_{tr}$  from the binary mixture samples upon heating and cooling as a function of temperature  $T$  during the  $N$ - $Sm-A$  and the  $Sm-A$ - $N$  transitions for the samples having different weight percentages of liquid-

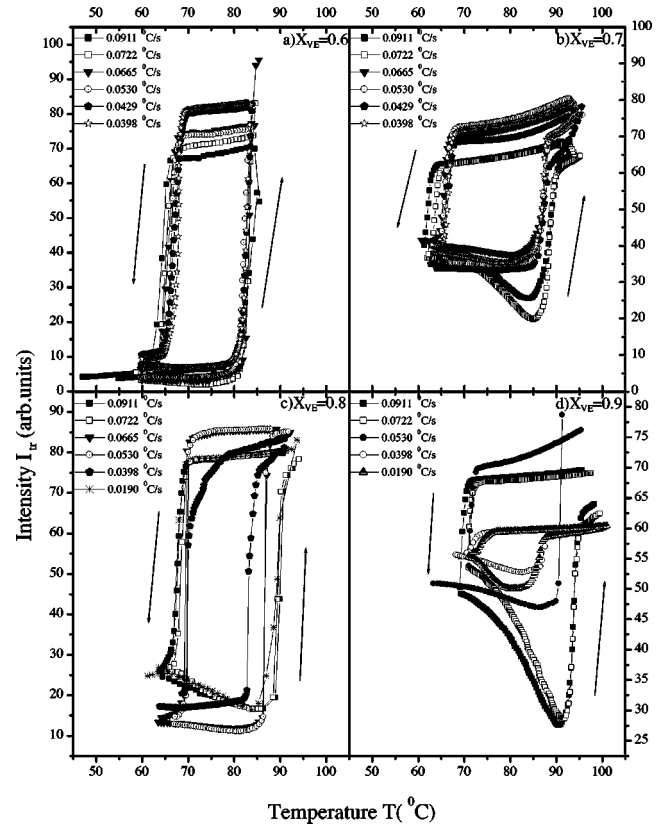


FIG. 3. The thermal hysteresis loops at various scan rates  $R$  for VE+AH mixtures (a)  $X_{VE}=0.6$ , (b)  $X_{VE}=0.7$ , (c)  $X_{VE}=0.8$ , (d)  $X_{VE}=0.9$ .

crystalline monomer VE.  $X_{VE}$  is defined as the weight percentage of VE in the binary mixture. The hysteresis loops have been obtained for the samples prepared with  $X_{VE}=0.6, 0.7, 0.8$ , and  $0.9$ . Temperature was driven linearly with prescribed scan rates  $R=0.02, 0.039, 0.043, 0.053, 0.067, 0.072$ , and  $0.091 \text{ } ^\circ\text{C}/\text{sec}$  and transmitted photon intensity measurements were repeated to produce the hysteresis loops at different  $R$  values. Figures 3(a)–3(d) show a family of hysteresis loops at different scan rates for various binary VE+AH mixtures. These results were reproducible, i.e., the maximum difference between any data points of the different runs was about 0.5%. In Fig. 3, it is seen that the areas of the hysteresis loops increase as the scan rate of the temperature is increased. In order to quantify these results, the areas  $A$  of the loops have been produced for different scanning rates  $R$  and compositions  $X_{VE}$ . The data were then fitted to the scaling form given in Eq. (2). In Table I, the scaling exponents  $n$  for different  $X_{VE}$  compositions are presented. As seen in Table I, the exponent  $n$  for  $X_{VE}=0.6$  and  $0.8$  samples is quite close to the value given by Zhong and Zhang in Ref. [11]; however, for  $X_{VE}=0.7$  and  $0.9$  samples there is a deviation from the value given in Ref. [11]. The scaling behavior of the loop areas for various  $X_{VE}$  compositions on a log-log scale is presented in Fig. 4, where it is clearly seen that all lines possess nearly the same slope. The average of the scaling exponent  $n$  was found to be  $0.692$ , which is in good agreement with the model in Ref. [11]

TABLE I. The scaling exponent  $n$  for various VE+AH mixtures [refer to Eq. (2)].

$X_{VE}$	$n$
0.6	$0.672 \pm 0.008$
0.7	$0.766 \pm 0.05$
0.8	$0.701 \pm 0.04$
0.9	$0.629 \pm 0.005$

within the experimental resolution. As seen Figs. 3(a)–3(d), it is worthwhile to note that the difference in the transmitted photon intensities of the nematic and smectic  $A$  phases arises since director fluctuations make the former turbid. In smectics twist and bend are expelled by the presence of a nonzero layer-compression modulus  $B$ , hence smectics are less turbid than nematics. In effect, the hysteresis measured is that of the layer-compression modulus  $B$ .  $B$  describes the elastic changes in the layer thickness. de Gennes has shown that  $B$  is proportional to the square of the magnitude of the smectic order parameter [26]. Furthermore, Zhong and Zhang also obtained the thermal hysteresis loops in the plane of the reduced temperature and its conjugate variable [11]. Their variable  $s$  conjugate to the reduced temperature is also proportional  $M^2$ . The areas of the hysteresis loops in the plane mentioned above obey the scaling relation given by Eq. (2) with  $n = 2/3$ . Since  $B \sim |\psi|^2$ , the hysteresis measured in this work is that of the conjugate variable  $I_{tr} \sim |\psi|^2$ . Here it should be noted that the scaling behavior is universal for the thermal hysteresis loops studied here. As shown in Fig. 3, the shape of the loops varies with binary compositions  $X_{VE}$ . For example, the loops for  $X_{VE} = 0.6$  and  $0.8$  are more symmetrical than the loops for  $X_{VE} = 0.7$  and  $0.9$  samples. Moreover, it

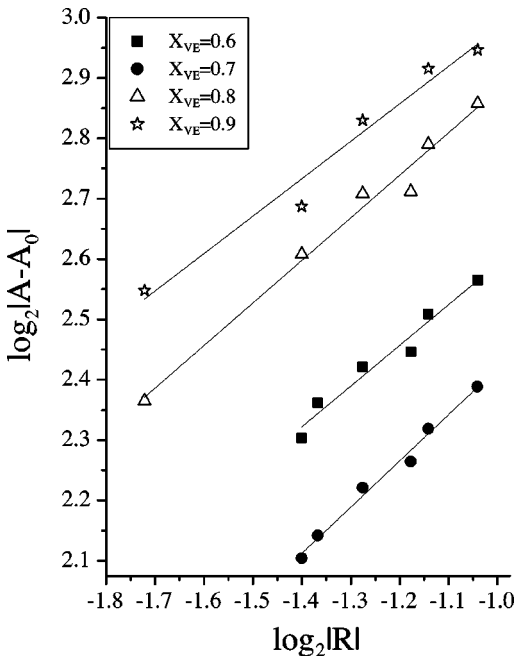


FIG. 4. Log-log plot of the area  $A$  versus temperature scanning rate  $R$ . Note that the constant term  $A_0$  has been subtracted to give straight lines.

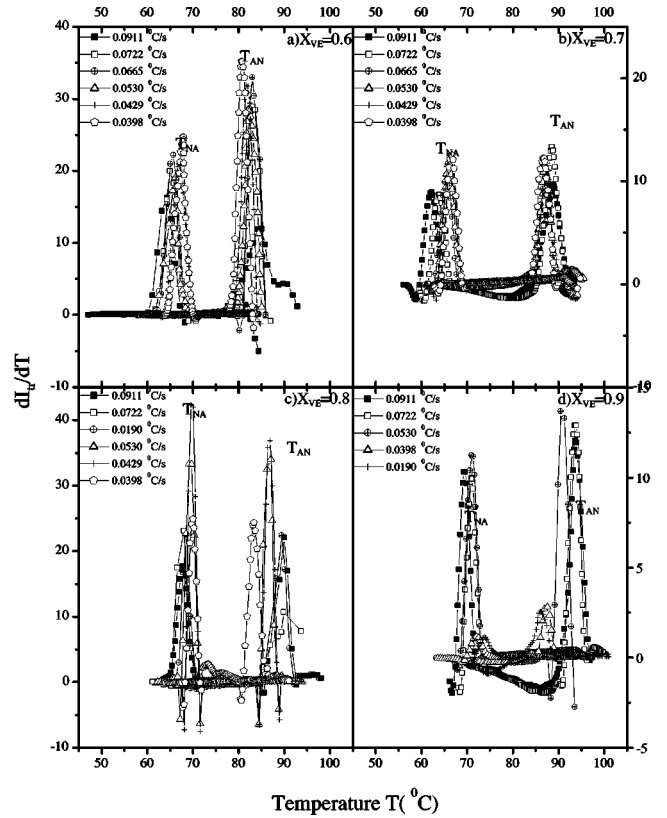


FIG. 5. The first derivative  $I_{tr}$  curves versus temperature at different temperature scanning rate for VE+AH mixtures (a)  $X_{VE} = 0.6$ , (b)  $X_{VE} = 0.7$ , (c)  $X_{VE} = 0.8$ , (d)  $X_{VE} = 0.9$ . The peak positions correspond to the  $T_{AN}$  and  $T_{NA}$  transition temperatures.

is worth noting that we observed a collapse of the hysteresis loops at a ‘‘critical’’  $X_{VE}^*$  composition, governed by the condition  $X_{VE} < X_{VE}^* = 0.6$ . Although the area of the hysteresis loops decreases as  $X_{VE}$  goes towards the tricritical point  $X_{VE} = 0.9$  [24], one is unable to observe any scaling relation between the areas of the loops and  $X_{VE}$  compositions. The scaling exponent  $n$  is found to be independent of composition  $X_{VE}$ .

Furthermore, it is possible to define the hysteresis width as  $\Delta T = |T_{AN} - T_{NA}|$  where  $T_{AN}$  and  $T_{NA}$  are the Sm-A-N (upon heating) and the N-Sm-A (upon cooling) transition temperatures, respectively. The  $T_{AN}$  and  $T_{NA}$  transition temperatures were determined from the peak positions of the first derivative of the  $I_{tr}(T)$  curves at different scan rates for each  $X_{VE}$  composition (see Fig. 5). It is interesting to investigate whether there is a scaling relation between the hysteresis width  $\Delta T$  and the scan rate  $R$ . The hysteresis width data obtained in this work over the entire range are consistent with the following scaling law

$$\Delta T \approx R^\beta, \tag{3}$$

where  $\beta$  is the scaling exponent. The scaling exponents are produced for each  $X_{VE}$  composition by fitting the  $\Delta T$  data to the double logarithmic form of Eq. (3). Log-log plots of the hysteresis width versus scan rate  $R$  for various VE+AH mixtures are shown in Fig. 6. Table II presents the produced

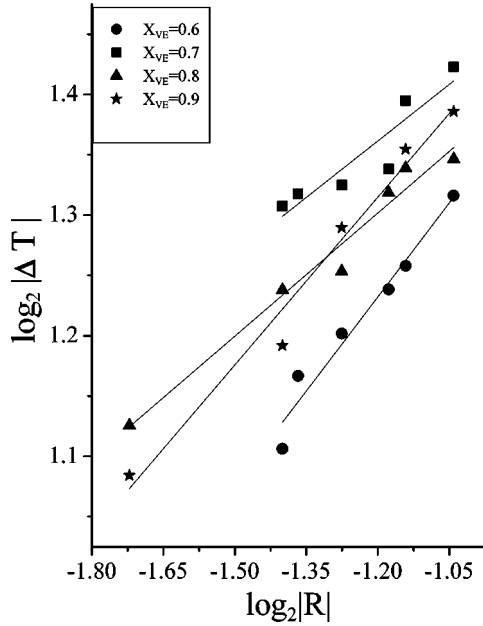


FIG. 6. Log-log plot of the hysteresis width  $\Delta T$  versus temperature scanning rate  $R$ . The solid lines are the double logarithmic fits of Eq. (3).

TABLE II. The scaling exponent  $\beta$  for various VE+AH mixtures [refer to Eq. (3)].

$X_{VE}$	$\beta$
0.6	$0.519 \pm 0.053$
0.7	$0.312 \pm 0.006$
0.8	$0.34 \pm 0.003$
0.9	$0.463 \pm 0.04$

scaling exponents  $\beta$  for  $X_{VE}=0.6, 0.7, 0.8$ , and  $0.9$  samples. The averaged scaling exponent was found to be  $0.409$ . Similar scaling relation between the hysteresis width and the scanning rate was reported by Toombes *et al.* [27] during the  $L_{\alpha}-H_{II}$  phase transition of fully-hydrated DOPE mixture. The value of the exponent  $\beta$  produced by Toombes *et al.* was approximately  $1/4$  which is nearly half of our result. Both the results of Toombes *et al.* and our results are experimental results. To the best of our knowledge there is no theoretical study, specifically based on field-theoretical models or model Hamiltonians, which gives this unexpected power-law relationship [Eq. (3)]. This behavior needs further investigation. As mentioned earlier, for  $X_{VE} < 0.6$  samples, the hysteresis loops cannot be obtained, since the hysteresis widths were narrower than the ones for the samples  $X_{VE} > 0.6$ . For instance, the hysteresis width is  $\Delta T = 0.94$  °C for  $X_{VE} = 0.4$

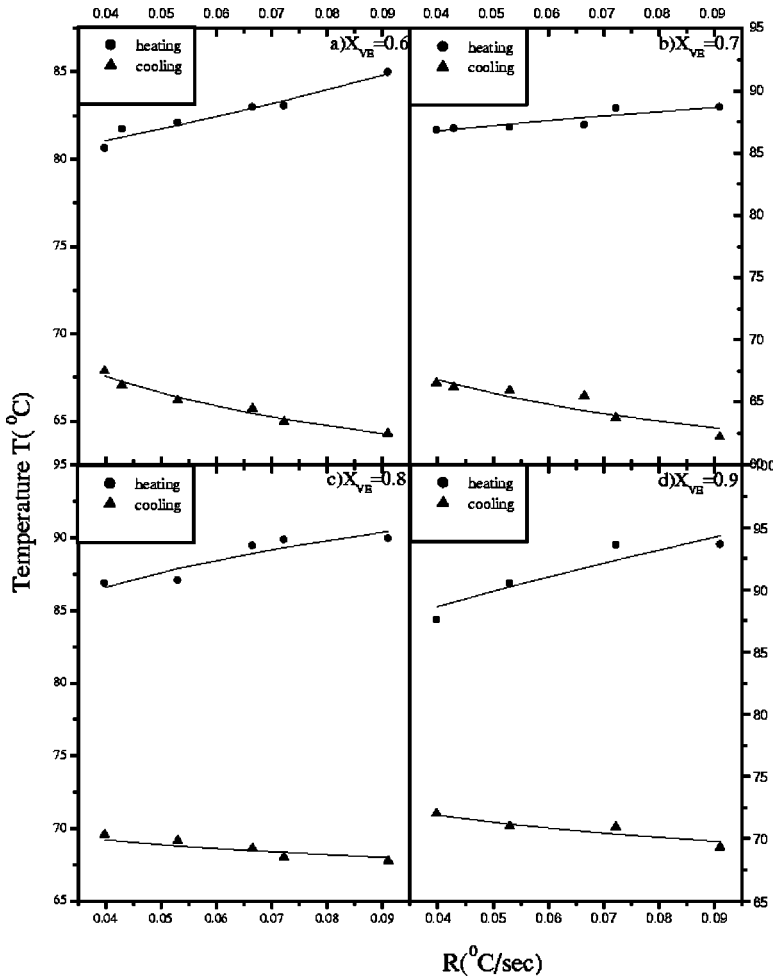


FIG. 7. The  $T_{AN}$  and  $T_{NA}$  transition temperatures versus temperature scan rate  $R$  for VE +AH mixtures (a)  $X_{VE}=0.6$ , (b)  $X_{VE}=0.7$ , (c)  $X_{VE}=0.8$ , (d)  $X_{VE}=0.9$ .

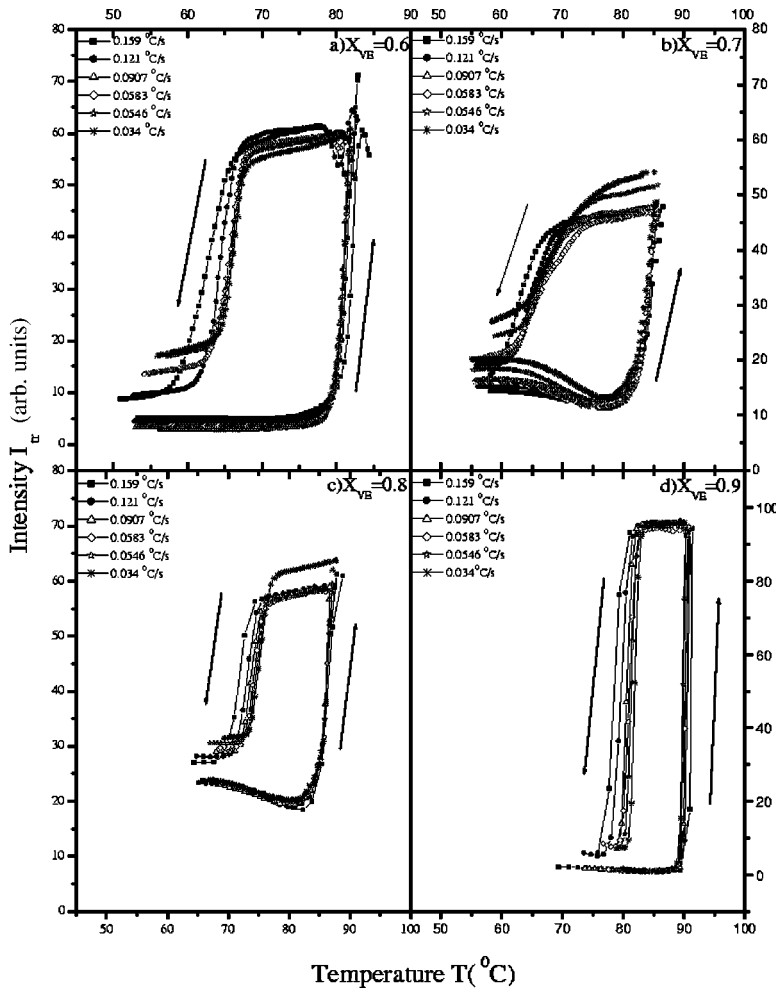


FIG. 8. The presaturation thermal hysteresis loops at various scan rates  $R$  below  $T_{AN}$  transition temperatures for mixtures (a)  $X_{VE}=0.6$ , (b)  $X_{VE}=0.7$ , (c)  $X_{VE}=0.8$ , (d)  $X_{VE}=0.9$ .

mixture. No scaling relation can be determined between the hysteresis width  $\Delta T$  and composition  $X_{VE}$  as mentioned previously for the areas and composition  $X_{VE}$ . Here it is also observed that the exponent  $\beta$  is nearly independent of  $X_{VE}$  values. It should be noted that the  $T_{AN}$  and  $T_{NA}$  transition temperatures are found to be dependent upon the rate at which the temperature is changed. We present the  $T_{AN}$  and  $T_{NA}$  temperatures as a function of the scan rate  $R$  for various VE+AH mixtures in Fig. 7, where it is apparent that the hysteresis width decreases as the scanning rate decreases as expected. For low scanning rates, the loop areas become smaller and the saturation in the transmitted photon intensity takes place faster (Fig. 3).

Finally, Fig. 8 shows partial hysteresis loop, where the heating branch is reversed before saturation. These runs suggest new scaling exponents. Furthermore, the loops do not merge at the end of the cooling branch, suggesting glassy behavior. These phenomena are under current investigation.

In conclusion, this work has presented the scaling behavior of thermal hysteresis during the  $N$ -Sm-A and the Sm-A- $N$  transitions in VE+AH system. We have obtained the thermal hysteresis loops under linearly varying temperature in the frame of the transmitted photon intensity and temperature. The area of the hysteresis loops increases with the temperature scanning rate and exhibits a scaling behavior [Eq. (2)] with an exponent equal to 0.692, which is in agreement with the  $(\Phi^2)^3$  model value within the experimental resolution. It is observed that the exponent is independent of composition  $X_{VE}$ .

#### ACKNOWLEDGMENTS

The authors wish to thank Professor I. E. Serhatlı for providing the AH and VE monomers. Ö.P. and A.N.B. thank the Academy of Sciences of Turkey for partial support.

- [1] M. Rao, H.R. Krishnamurthy, and R. Pandit, Phys. Rev. B **42**, 856 (1990).  
 [2] M. Rao and R. Pandit, Phys. Rev. B **43**, 3373 (1991).  
 [3] W.S. Lo and R.A. Pelcovits, Phys. Rev. A **42**, 7471 (1990).

- [4] D. Dhar and P.B. Thomas, J. Phys. A **25**, 4967 (1990).  
 [5] S. Sengupta, Y. Marathe, and S. Puri, Phys. Rev. B **45**, 7828 (1992).  
 [6] D. Dhar and P.B. Thomas, Europhys. Lett. **21**, 965 (1993).

- [7] A.M. Somoza and R.C. Desai, *Phys. Rev. Lett.* **70**, 3279 (1993).
- [8] M. Ackaryya and B.K. Chakrabarti, *Physica A* **192**, 471 (1993).
- [9] C.N. Luse and A. Zangwill, *Phys. Rev. E* **50**, 224 (1994).
- [10] F. Zhong, J.X. Zhang, and G.G. Siu, *J. Phys.: Condens. Matter* **6**, 7785 (1994).
- [11] F. Zhong and J.X. Zhang, *Phys. Rev. E* **51**, 2898 (1995).
- [12] P. Jung, G. Gray, R. Roy, and P. Mandel, *Phys. Rev. Lett.* **65**, 1873 (1990).
- [13] Y.L. He and G.C. Wang, *Phys. Rev. Lett.* **70**, 2336 (1993).
- [14] C.E. Lee and S.H. Yang, *J. Korean Phys. Soc.* **33**, L635 (1998).
- [15] S. Sarmiento, P.S. Carvalho, M.R. Charves, F. Pinto, and H.T. Nguyen, *Liq. Cryst.* **28**, 1839 (2001).
- [16] P.J. Wu, Y.C. Shen, Y.H. Liu, C.R. Lo, A.J. Jin, C.C. Huang, and C.Y. Chao, *Chin. J. Phys. (Taipei)* **38**, 471 (2000).
- [17] W.H. Weng, J.L. Chen, Z.H. Liu, G.H. Wu, and W.S. Zhan, *Phys. Rev. B* **65**, 012416 (2001).
- [18] S. Kara, C. Tamerler, H. Bermek, and Ö. Pekcan, *Int. J. Biol. Macromol.* **31**, 177 (2003).
- [19] S. Kara, C. Tamerler, H. Bermek, and Ö. Pekcan, *J. Bioactive Compatible Polym.* **18**, 33 (2003).
- [20] H. Özbek, S. Yıldız, and Ö. Pekcan, *Phys. Rev. E* **59**, 6798 (1999).
- [21] H. Özbek, S. Yıldız, Ö. Pekcan, and A.N. Berker, *Int. J. Mod. Phys. B* **15**, 2161 (2001).
- [22] H. Özbek, S. Yıldız, Ö. Pekcan, Y. Hepuzer, Y. Yağcı, and G. Galli, *Mater. Chem. Phys.* **78**, 318 (2002).
- [23] A.S. Angeloni, D. Garetti, M. Laus, E. Chiellini, and G. Galli, *J. Polym. Sci. A* **29**, 1865 (1991).
- [24] E. Chiellini, G. Galli, M.C. Bignozzi, A.S. Angeloni, M. Fagnani, and M. Laus, *Macromol. Chem. Phys.* **196**, 3187 (1995); I.E. Serhatlı and M. Serhatlı, *Turk J. Chem.* **22**, 279 (1998), and references cited therein.
- [25] S. Yıldız, I.E. Serhatlı, Ö. Pekcan, A.N. Berker, and H. Özbek, *Int. J. Mod. Phys. B* **16**, 3959 (2002).
- [26] P.G. de Gennes and J. Prost, *The Physics of Liquid Crystals*, 2nd ed. (Oxford University Press, Oxford, 1993).
- [27] G.E.S. Toombes, A.C. Finnefrock, M.W. Tate, and S.M. Gruner, *Biophys. J.* **82**, 2504 (2002).